



## Easily synthesized soybean oil bio-based material for wastewater treatment<sup>☆</sup>

Viviana Barra<sup>a,1</sup>, Elena Piacenza<sup>b,1</sup>, Sara Amata<sup>b</sup>, Salvatore Martino<sup>a</sup>, Filippo Vitale<sup>b,c</sup>,  
 Delia Francesca Chillura Martino<sup>b</sup>, Silvestre Buscemi<sup>b</sup>, Carla Rizzo<sup>b,\*</sup>,  
 Antonio Palumbo Piccionello<sup>b,\*</sup>

<sup>a</sup> Department of Biological, Chemical and Pharmaceutical Sciences and Technologies, section of Cellular Biology Italy, University of Palermo, Viale delle Scienze, Ed. 16, 90128 Palermo, Italy

<sup>b</sup> Department of Biological, Chemical and Pharmaceutical Sciences and Technologies, section of Chemistry Italy, University of Palermo, Viale delle Scienze, Ed. 17, 90128 Palermo, Italy

<sup>c</sup> Department of Pharmacy, University of Copenhagen, Universitetsparken 2, Copenhagen DK-2100, Denmark

### ARTICLE INFO

#### Keywords:

Soybean oil  
 Bio-based materials  
 Green synthesis  
 Environmental remediation  
 Wastewater pollution

### ABSTRACT

The need for alternative petroleum-based polymers sheds light on developing new biomaterials, even though their synthesis frequently has an enormous environmental impact. Hence, a new synthetic approach to prepare simple soybean oil (SO) derived materials is here proposed to decrease the polymerization impact. Fresh and expired SO are used as starting materials, and a solid gummy material is obtained using BF<sub>3</sub> as catalyst in just 1 h with microwave irradiation. A combined approach of <sup>1</sup>H NMR, GC-MS, and ATR-FTIR analyses enabled an understanding of the principal role of the fatty acids' unsaturation on the cross-linking reaction. The material was characterized through SEM, DSC, nanotomography and XRD analyses, revealing a compact morphology with some cavities. The material was, then, applied as adsorbent for some wastewater pollutants. Adsorption efficiencies of the bio-based material for different organic solvents or dye water solution were analysed, obtaining good efficiencies. Moreover, the material can be recycled after pollutant adsorption and used several times. Finally, it can be chemically degraded and is biocompatible, expanding the application of this bio-based material also to other fields.

### 1. Introduction

The environmental pollution due to solid waste has been rapidly growing with the extensive use of petroleum-based plastics. Hence, the depletion of fossil sources and the problematic degradation of petroleum-based plastic have pushed researchers and industry to fully investigate natural biopolymers derived from microorganisms, plants, trees or bio-based polymer synthesized from biomass waste or biological sources i.e. vegetable oils, sugars, fats, resins, proteins, amino acids [1]. In this framework, “green polymers” can be classified as “bio-replacement” or as “bioadvantaged” polymers [2]. Bioadvantaged polymers are formed by new monomers different from petroleum derived ones and can be synthesized through modifications of natural sources. This synthetic strategy yields new molecules with unexplored

properties that can represent a valid alternative to petrochemical polymers.

For example, vegetable oils are powerful starting materials thanks to the presence of unsaturated fatty acids in triglycerides structures. Unsaturated fatty acids possess at least one carbon-carbon double bond that can be used to synthesize materials with little chemical modification [3]. Usually, the oleic and linolenic acid chains are situated on the C2 carbon of the glycerol, which renders them less sterically accessible, preventing their natural polymerization. For this reason, chemical modifications such as double bond isomerization, epoxidation [4] and subsequent ring opening reaction for condensation have been successfully performed [5].

The cationic polymerization of vegetable oils using BF<sub>3</sub>·Et<sub>2</sub>O was extensively studied by Lu and Larock, however thermosets polymers

<sup>☆</sup> **Dedication:** in memory of Prof. Richard G. Weiss great scientist and mentor.

\* Corresponding authors.

E-mail addresses: [carla.rizzo03@unipa.it](mailto:carla.rizzo03@unipa.it) (C. Rizzo), [antonio.palumbopiccionello@unipa.it](mailto:antonio.palumbopiccionello@unipa.it) (A. Palumbo Piccionello).

<sup>1</sup> These authors contribute equally.

obtained under their conditions did not find any application. Instead, they copolymerized vegetable oils with petroleum derivatives such as styrene, divinylbenzene and other analogues for several applications [3,5,6]. In general, thermosets polymers derived from vegetable oils showed poor material performances [7], for this reason acrylation [8], transesterification [9] and co-polymerization [10] strategies have been adopted to improve oil-derived thermoset polymers properties. All these modifications can be also easily performed on epoxidized vegetable oils instead of natural oils [11]. For example, some soybean-oil-based epoxy acrylate resins, developed via a ring-opening reaction of epoxidized soybean oil (ESO) showed good volatility and mechanical strength allowing their application in UV-curable coatings [12]. Following this strategy, also new ESO-based copolymers and doped polymers were prepared for potential biomedical applications, thanks to their nontoxic and biocompatible nature [13,14]. Furthermore, a combination of multiple bio-based starting materials has been recently used to synthesize new biopolymers with superior thermal, mechanical properties and degradability [15,16].

Nevertheless, the direct conversion of pure natural vegetable oils in valuable materials and their possible applications have been poorly investigated. However, the direct conversion of vegetable oils could drastically decrease the environmental impact of the synthetic pathway. For this reason, a new synthetic approach is here developed to obtain a soybean oil gummy solid (SOGS). The overall impact of the process is decreased with microwave assisted synthesis and minimizing the amount of catalyst (Scheme 1). In addition, being awarded that the higher porosity, surface area, and processing efficiency of bio-based materials make easier the removal of several pollutants [17,18], the soybean oil (SO) derived material has been used as adsorbent for preliminary analysis in environmental remediation, seldom investigated to this aim [19].

The chemical composition and physical-chemical structure of the material have been analysed through  $^1\text{H}$  NMR, GC-MS, XRD and ATR-FTIR approaches. Material properties such as swelling ability, chemical degradation, thermal stability and morphology were investigated as well. In particular, the last two properties were analysed through differential scanning calorimetry (DSC), scanning electron microscopy (SEM) and nanotomography techniques. SOGS adsorption ability in wastewater solutions polluted by organic dyes and halogenated solvents

such as chloroform has been analysed as well, alongside the recycling ability of the material after pollutant desorption. Finally, the biocompatibility of the material has been also investigated through in vitro cytotoxicity and cell viability assays on normal human epithelial cell cultures.

## 2. Materials and methods

Soybean oil, olive oil, linoleic acid technical, 58–74 % (GC), oleic acid technical, 90 % (GC), Boron trifluoride diethyl etherate, rhodamine B (RhB), sodium hydroxide, potassium hydroxide, sodium bicarbonate, chloroform, methanol and all solvents were purchased from commercial source and used without any further purifications. Expired soybean oil was purchased from a local market and stored 6 years above the expiring date at room temperature.

**Cell culture:** Retinal Pigment Epithelial cells (RPE-1), h-TERT immortalized, were cultured in Dulbecco's modified Eagle's medium (DMEM; Corning) supplemented with 10 % bovine foetal serum and 1 % L-Glutamine. Cells were grown at 37 °C in a humidified atmosphere with 5 %  $\text{CO}_2$ .

$^1\text{H}$  NMR were recorded on a Bruker instrument operating at 400 MHz and using residual peaks solvents as references.

A lyophilizer Scanvac Cool Safe operating at  $-90$  °C was used to eliminate residual solvent traces on samples.

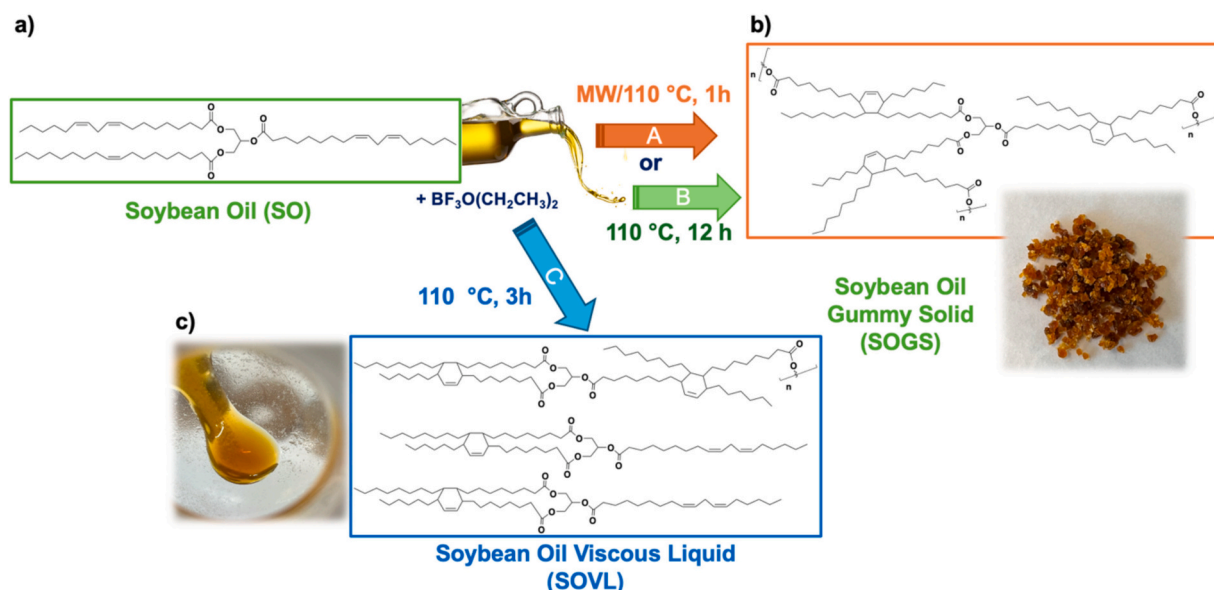
### 2.1. Synthetic procedures

#### 2.1.1. Synthesis of (SOGS)

100  $\mu\text{L}$  of  $\text{BF}_3 \cdot \text{Et}_2\text{O}$  were added to 2 g of SO in a sealed tube. The reaction mixture was stirred at room temperature for 3 h and afterwards at 110 °C for 12 h. A brown solid was obtained, and it was washed first with hexane ( $3 \times 15$  mL), then with a  $\text{NaHCO}_3$  saturated water solution ( $3 \times 15$  mL) and finally with ultra-pure water until neutral pH was reached. 1.6 g of a light brown gummy solid was obtained after lyophilization.

#### 2.1.2. Synthesis of (SOGS) under MW

For microwave synthesis a Start Synth oven equipped with a sealed tube has been used.



**Scheme 1.** Schematic representation of cross-linking reaction of SO in different reaction conditions (A: under microwave irradiation for 1 h, B: normal heat for 12 h, C: normal heat for 3 h). a) Representative Soybean Oil (SO) structure and picture, b) representative Soybean Oil Gummy Solid (SOGS) structure and picture, showing possible intermolecular adducts after triglycerides cross-linking reaction, c) representative Soybean Oil Viscous Liquid (SOVL) structure and picture, showing possible intramolecular and intermolecular adducts after triglycerides partial cross-linking reaction. Polymer structures are depicted as visual aid.

100  $\mu\text{L}$  of  $\text{BF}_3 \cdot \text{Et}_2\text{O}$  were added to 2 g of SO in a MW tube with a stirring bar and weflon button. The reaction mixture was stirred at 110  $^\circ\text{C}$  for 1 h with a maximum power of 300 W, to reach this temperature a ramp from room temperature to 110  $^\circ\text{C}$  for 10 min was set with a maximum power of 300 W. A brown solid was obtained, it was washed first with hexane ( $3 \times 15 \text{ mL}$ ), then with a  $\text{NaHCO}_3$  saturated water solution ( $3 \times 15 \text{ mL}$ ) and finally with ultra-pure water until neutral pH was reached. 1.6 g of a light brown gummy solid was obtained after lyophilization.

### 2.1.3. Synthesis of (SOVL)

100  $\mu\text{L}$  of  $\text{BF}_3 \cdot \text{Et}_2\text{O}$  were added to 2 g of SO in a sealed tube. The reaction mixture was stirred at room temperature for 3 h and afterwards at 110  $^\circ\text{C}$  for 3 h. A viscous liquid was obtained, and it was solubilized in hexane to wash in separation funnel with a  $\text{NaHCO}_3$  saturated water solution ( $3 \times 15 \text{ mL}$ ) and finally with ultra-pure water until neutral pH was reached. Organic phase was anhydriified with  $\text{Na}_2\text{SO}_4$  and then solvent was removed with rotavapor under reduced pressure. A light orange viscous oil was obtained.

### 2.1.4. Synthesis of (OOVL)

100  $\mu\text{L}$  of  $\text{BF}_3 \cdot \text{Et}_2\text{O}$  were added to 2 g of OO in a sealed tube. The reaction mixture was stirred at room temperature for 3 h and afterwards at 110  $^\circ\text{C}$  for 3 h. A viscous liquid was obtained, and it was solubilized in hexane to wash in separation funnel with a  $\text{NaHCO}_3$  saturated water solution ( $3 \times 15 \text{ mL}$ ) and finally with ultra-pure water until neutral pH was reached. Organic phase was anhydriified with  $\text{Na}_2\text{SO}_4$  and then solvent was removed with rotavapor under reduced pressure. A light brown viscous oil was obtained.

### 2.1.5. Synthesis of methyl esters of fatty acids and materials for GC–MS analysis

100 mg of oils or solid were weighed in a pyrex tube and 2 mL of 1 % of methanolic solution of NaOH were subsequently added. The reaction mixture was stirred for 15 min at 55  $^\circ\text{C}$ . Then, 4 mL of methanolic solution of HCl (4 %) was added to the reaction mixture and it was stirred for further 15 min at 55  $^\circ\text{C}$ .

After cooling of the solution, methyl esters extraction was carried out adding 2 mL of water and 4 mL of hexane, the organic layer was separated from water phase and further 2 extractions were performed with hexane. 1 mL of organic phase was analysed with GC–MS with triple quadrupole GC/MS Agilent 7010. Measurements were performed using a ramp temperature of 2  $^\circ\text{C}/\text{min}$  from 40  $^\circ\text{C}$  to 250  $^\circ\text{C}$ , temperature kept for 15 min. Then a ramp temperature of 10  $^\circ\text{C}/\text{min}$  was used to reach 270  $^\circ\text{C}$ , temperature kept for 20 min.

The GC–MS mass spectrum data were analysed using MassHunter Qualitative Analysis B.06.00, and the database of the National Institute Standard and Technology (NIST) was used to identify the corresponding fatty acids.

## 2.2. ATR-FTIR spectroscopy

ATR-FTIR spectroscopy was performed as described elsewhere [20]. Briefly, an FTIR Bruker Vertex 70v Advanced Research (Bruker, Billerica, MA, USA) equipped with a platinum ATR and a diamond crystal ( $\eta = 2.4$ ) was used to collect spectra in the 3800–600  $\text{cm}^{-1}$  range, with a later resolution of 2  $\text{cm}^{-1}$  and 180 scans *per* sample. A baseline correction of scattering was made in all ATR-FTIR spectra, which were analysed using the OPUS 7.5® and OriginPro software.

## 2.3. XRD analysis

XRD pattern of SOGS was acquired with a Bruker ecoD8 ADVANCE (Bruker, Billerica, MA, USA) instrument working in the  $\theta$ -2 $\theta$  geometry equipped with a Cobalt tube ( $\lambda = 1.79 \text{ \AA}$ ) and a LynxEye detector (1D mode) [20]. The pattern was collected in the 2 $\theta$  range of 5–55 $^\circ$  (setup

conditions: 40 kV tube voltage, 25 mA current, 0.02 $^\circ/\text{s}$ ) and analysed using Match! 3 and OriginPro software. The degree of crystallinity for the SOGS was also calculated by using the Match! 3 software.

## 2.4. Nanotomography and SEM imaging

Nanotomography and SEM imaging were performed on the SOGS. For nanotomography, a Microtac Micro-CT Skyscan 1272 (Bruker, Billerica, MA, USA) was used with a voxel size of 500 nm and an X-ray voltage of 40 kV.

SEM imaging and single-point elemental analysis were performed by depositing a small piece of SOGS onto the aluminum stab via carbon tape and using a Desktop SEM Phenom PRO X (ThermoFisher Scientific, Milan, IT) equipped with an EDX detector at an accelerating voltage of 15 kV.

## 2.5. DSC analysis

Differential scanning calorimetry (DSC) measurements were carried out with a TA Instruments mod. 2920 Differential Scanning Calorimeter (TA Instrument Inc., New Castle, DE, USA) equipped with a TA Instruments Refrigerated Cooling System. Samples (~4 mg) were weighed in aluminum TA Tzero Hermetic Pans, which were subsequently sealed with aluminum lids. The analysis was performed with heating and cooling rates of 10  $^\circ\text{C}/\text{min}$  under a  $\text{N}_2$  atmosphere of 50  $\text{mL min}^{-1}$ . Three heating and cooling ramps were carried out in a temperature range between 0  $^\circ\text{C}$  and 300  $^\circ\text{C}$ .

## 2.6. Swelling tests

20 mg of SOGS were weighed in a screw-capped vial and 1.5 mL of the desired solvents were added and left in contact for 24 h. After that time, solvent was removed, and the wet solid was weighed to calculate the % of swelling (Q) as in the Eq. 1:

$$Q = \frac{m_{(\text{wet})} - m_{(\text{dry})}}{m_{(\text{dry})}} \quad (1)$$

where  $m_{(\text{wet})}$  is wet SOGS mass,  $m_{(\text{dry})}$  is dry SOGS mass that is the initial mass.

## 2.7. Dye adsorption tests

In a screw-capped vial, 20 mg of SOGS were suspended in 1.5 mL of different dye solution in water ( $1.8 \cdot 10^{-5} \text{ M}$ ). After 24 h of contact, the water solution was withdrawn for UV analysis, performed using quartz cuvette with optical wavelength of 1 cm with UV Analytik Jena Specord S600, interfaced with Winaspect software.

Concentrations of water dye solutions after contact with the material were calculated using a calibration curve. For RhB, a calibration curve in the range  $1.6 \times 10^{-6} - 1.8 \times 10^{-5} \text{ M}$  was determined following the maximum absorption band at 554 nm. Adsorption efficiency was calculated according to Eq. 2, where  $C_0$  is the initial RhB concentration and  $C_t$  is the final concentration after adsorption:

$$E (\%) = \frac{C_0 - C_t}{C_0} \times 100 \quad (2)$$

For material adsorption kinetic, different times of contact between SOGS and dye solutions were set. Different amounts of SOGS were put in contact with the same volume and concentration of RhB solutions (1.5 mL and  $1.8 \cdot 10^{-5} \text{ M}$ ) to test the maximum capacity of adsorption of the material.

## 2.8. Dye desorption from SOGS and recycling tests

Desorption tests were performed on SOGS loaded (20 mg) with RhB

adsorbed on it after 24 h, using EtOH or 2-Me-THF and sonication for 10 min ( $3 \times 1.5$  mL). After desorption, SOGS was dried in the oven at  $60^\circ\text{C}$  and then used again with fresh RhB for 24 h ( $1.5$  mL  $1.8 \times 10^{-5}$  M). Efficiency was calculated as described above.

## 2.9. Chloroform adsorption tests

In a screw-capped vial, 40 mg of SOGS were suspended in 1.5 mL of a water solution of  $\text{CHCl}_3$  (8 mg/mL). After different times of contact, 1 mL of water solutions was withdrawn and put in vials for solid-phase microextraction (SPME) for SPME-GC-MS analysis.

Residual  $\text{CHCl}_3$  concentrations were determined through a calibration curve in the range 0.1–8 mg/mL, using Eq. 2.

GC/MS analysis was performed by adapting previously reported methods [21].  $\text{CHCl}_3$  was extracted from water solution in the sealed vial headspace and concentrated using SPME before desorption in the GC injection port. Headspace extraction was performed with a 2.5 mL Syringe-HS (0.64–57-R-H, PTFE, GERSTEL) conditioned and held at  $40^\circ\text{C}$  from sample collection to injection.

In the SPME, one Fiber Assembly was evaluated and used: 50/30  $\mu\text{m}$  divinylbenzene (DVB)/carbowax (CAR)/polydimethylsiloxane (PDMS) (Supelco, Bellefonte, PA, USA). The fiber was exposed to chloroform solution in a 20 mL SPME vial ( $75.5 \times 22.5$  mm) for 10 min at  $40^\circ\text{C}$  after 10 min of equilibration time. The desorption time was 5 min. Before use, the fiber was conditioned and cleaned at  $270^\circ\text{C}$  for 30 min, following the instructions from Supelco®. Split of  $20$  mL  $\text{min}^{-1}$  injection was used.

Gas chromatographic analysis was performed using an Agilent 7000C GC (Agilent Technologies, Inc., Santa Clara, CA, USA) system equipped with a split/splitless injector, fitted with an Agilent HP5-MS UI capillary column ( $30$  m  $\times$   $250$   $\mu\text{m}$ ;  $0.25$   $\mu\text{m}$  film thickness) coupled to an Agilent triple quadrupole Mass Selective Detector MSD 5973 (Agilent Technologies, Inc., Santa Clara, CA, USA), with ionization voltage of 70 eV; electron multiplier energy of 2000 V; and transfer line temperature of  $270^\circ\text{C}$ . The solvent Delay was 0 min. Helium was used as the carrier

$$\% \text{Viability} = \frac{\text{Optical density of cells treated with SOGS} - \text{optical density of background}}{\text{Optical density of cells non treated with SOGS} - \text{optical density of background}} \quad (5)$$

gas ( $1$  mL  $\text{min}^{-1}$ ). The oven program was as follows: the temperature was initially kept at  $40^\circ\text{C}$  for 5 min and then gradually increased to  $200^\circ\text{C}$  at a rate of  $15^\circ\text{C}/\text{min}$ , which was held for 5 min. Samples were injected at  $200^\circ\text{C}$  automatically. The interval scan was 35–450  $m/z$  and the scan speed were  $10,000$   $\text{amu}\cdot\text{s}^{-1}$  (25 Hz).

## 2.10. Chemical degradation

To 100 mg of SOGS were added 2 mL of methanolic or water solution of NaOH (1 wt%) in a pyrex tube. The mixture was stirred for 16 h at  $60^\circ\text{C}$ .

Alternatively, to 50 mg of SOGS were added 12.5 mL of water solution of NaOH (2 M) or KOH (2 M) or HCl (2 M) in a pyrex tube. The mixture was stirred for 16 h at  $60^\circ\text{C}$ .

Then the mixture was filtered, and the solid residue was weighted to calculate the chemical degradation % (D), following Eq. 3:

$$D (\%) = \frac{m_i - m_f \times 100}{m_f} \quad (3)$$

where  $m_i$  is the initial mass (mg) of SOGS before the degradation treatment,  $m_f$  is the final mass (mg) of SOGS after the degradation treatment.

## 2.11. Cell proliferation analysis

Cells were seeded in a 12 multiwell at low density without (control) or with (treatment) SOGS in different amounts (0.8 mg, 1.6 mg, 2.4 mg or 5 mg in 1 mL culture media). For the conditioned media treatment, 5 mg SOGS were incubated in 1 mL culture media for 3 days and then the filtered media was used to treat the cells. Palmitic acid (1 mg in 1 mL culture media) was used to compare the toxicity of SOGS (5 mg in 1 mL).

After the treatments, cells were harvested by trypsinization, recovered in a tube and resuspended with Trypan Blue in a 1:1 ratio. Cell counting was performed manually using a Burkner Chamber as previously done [22]. To evaluate the number of cell population doublings the following formula (4) was used:

$$\text{Number of cell doublings} = \ln(\text{fold increase in cell number}) / \ln 2 \quad (4)$$

## 2.12. MTT assay

Cell viability was assessed by using 3-(4,5-dimethylthiazole-2-yl)-2,5-diphenyltetrazoliumbromide (MTT). MTT reagent was prepared by dissolving MTT (Vybrant MTT Cell Proliferation Assay kit V-13154; Life technologies) in 1 mL PBS (MTT stock solution 5 mg/ml). Cells were seeded in a 96-well plate at a density of 2500 cells/well in 200  $\mu\text{L}$  of culture medium. Additionally, one well was left empty to evaluate the cell-free background. The cells were then treated with 800  $\mu\text{g}$ , 1600  $\mu\text{g}$ , 2400  $\mu\text{g}$  SOGS for 24 h. The day of the analysis, the media was changed with a 110  $\mu\text{L}$  PBS + MTT solution (100  $\mu\text{L}$  PBS + 10  $\mu\text{L}$  MTT stock solution). After 4 h of incubation in the dark at  $37^\circ\text{C}$ , MTT solution was removed, and the cells were washed with PBS. Finally, the DMSO was added to each well and the absorbance was measured using a microplate reader Biotek synergy HT at 540 nm after 10 min of incubation. All the treatment conditions were performed in triplicate. The percentage of viable cells was measured as follows, according to Eq. (5):

## 3. Results and discussion

### 3.1. Material synthesis

A small amount of Lewis acid (5 wt%) was added to a fresh or expired SO as described in Materials and Methods. The expired SO was a commercial SO expired 6 years ago and it showed comparable GC profile as fresh SO. The reaction mixture was stirred at room temperature for 3 h and then heated at  $110^\circ\text{C}$  overnight; a light brown gummy solid was obtained (Scheme 1). The same material was obtained in just 1 h when the reaction mixture was directly irradiated in a microwave reactor at the same temperature using a maximum power of 300 W and a quartz vessel. Bio-based material was obtained with both procedures with the same reaction yields, in addition its characterization confirmed the identical chemical composition and the same physical properties (see NMR spectra in Supplementary material).

The reaction was also carried out using olive oil (OO) or pure unsaturated fatty acids (linoleic and oleic acids, constituents of SO triglyceride) as starting materials and with SO in absence of the catalyst as well. Although the solid gummy material was not formed in any of these cases, these reactions allow the understanding of SO reactivity, favoring the reaction. In addition, SO reaction was also performed only for 3 h at

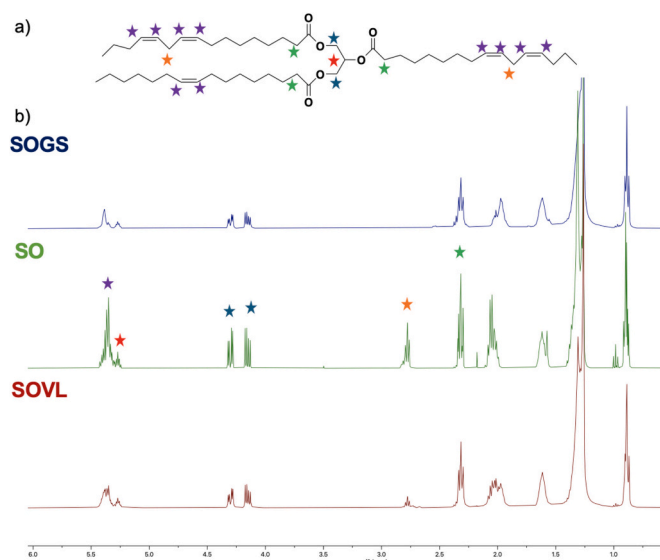


**Fig. 1.** a) Representative SO triglyceride structure; b) from up to the bottom,  $^1\text{H}$  NMR spectra in  $\text{CDCl}_3$  with peak assignment of SOGS soluble residue (upper blue), SO (middle in green), SOVL (bottom red).

110 °C with conventional heating, in these conditions a more viscous and brown oil (soybean oil viscous liquid, SOVL) was obtained instead of the solid gummy material (Scheme 1c).

The cationic polymerization of vegetable oils using  $\text{BF}_3 \cdot \text{Et}_2\text{O}$  was extensively used for copolymerization of vegetable oils with other petroleum sources. The reaction mechanism usually proceeds through the protonation of vinyl moieties in the triglycerides and subsequent polymerization as described for alkene reactions [6]. However, in some cases an intermediate formation of a Diels Alder adduct has been reported [23]. To shed light on the driving forces of the reaction, a combined approach of  $^1\text{H}$  NMR (Fig. 1 and Supplementary Materials) and GC-MS analysis of starting materials and different product reactions was applied.

$^1\text{H}$  NMR spectrum of SO revealed the average presence of 5 unsaturations in the triglyceride structures at 5.3–5.4 ppm (spectrum in the middle of Fig. 1b, NMR spectra in Supplementary Material). These signals can be ascribed to the general presence of 2 units of linoleic and 1 of oleic acid in SO triglyceride as shown in Fig. 1a [24]. The multiplet at 5.2 ppm diagnostic of CH glycerol unit, the peaks in the range 4.2–4.4 ppm diagnostic of  $\text{CH}_2$  glycerol unit, and the triplet at 2.3 ppm diagnostic of  $\text{CH}_2$  fatty acid directly linked to the carboxylic group confirm the ester functionality.

SOVL and SOGS spectra show a decrease of integrals for vinylic protons, corresponding to 2.5 and 1.5 unsaturations respectively. A decrease of bis-allylic protons can be observed also for SOVL, while a complete loss of this signal is observed for SOGS (upper spectrum of Fig. 1b, NMR spectra in Supplementary Material). This analysis confirmed that the reaction occurs through the vinylic reactivity with the Lewis acid. Moreover, the absence of signals related to  $\text{CH-O}$  protons in the 3–4 ppm region, exclude the radical polymerization with oxygen that produces the classical oil drying process [25].

GC-MS analysis performed on methyl-esters derived from SO and obtained materials (Fig. 2, Table 1) provides others insight on the reaction.

Fig. 2 shows the chromatograms and structures of SO methyl esters and of derived materials. All chromatograms show the peaks of saturated fatty acids, palmitic and stearic, at the retention times of 19.5 and

**Table 1**  
Retention times, fatty acids as components of methyl esters and relative percentages of SO and SO derived materials.

Retention time (min)	Fatty acids in methyl esters	MeSO	MeSOVL	MeSOGS
19.5	Palmitic acid (16:0)	8.8 %	17.4 %	28.3 %
27.0	Linoleic acid (18:2) cis, cis- $\Delta^{9,12}$	54.6 %	24 %	–
27.4	Oleic acid (18:1) cis- $\Delta^9$	32.5 %	27.7 %	12.8 %
27.8	6-Octadecenoic acid (18:1) cis- $\Delta^6$	–	26.0 %	49.2 %
28.8	Stearic acid (18:0)	4.1 %	4.9 %	7.7 %

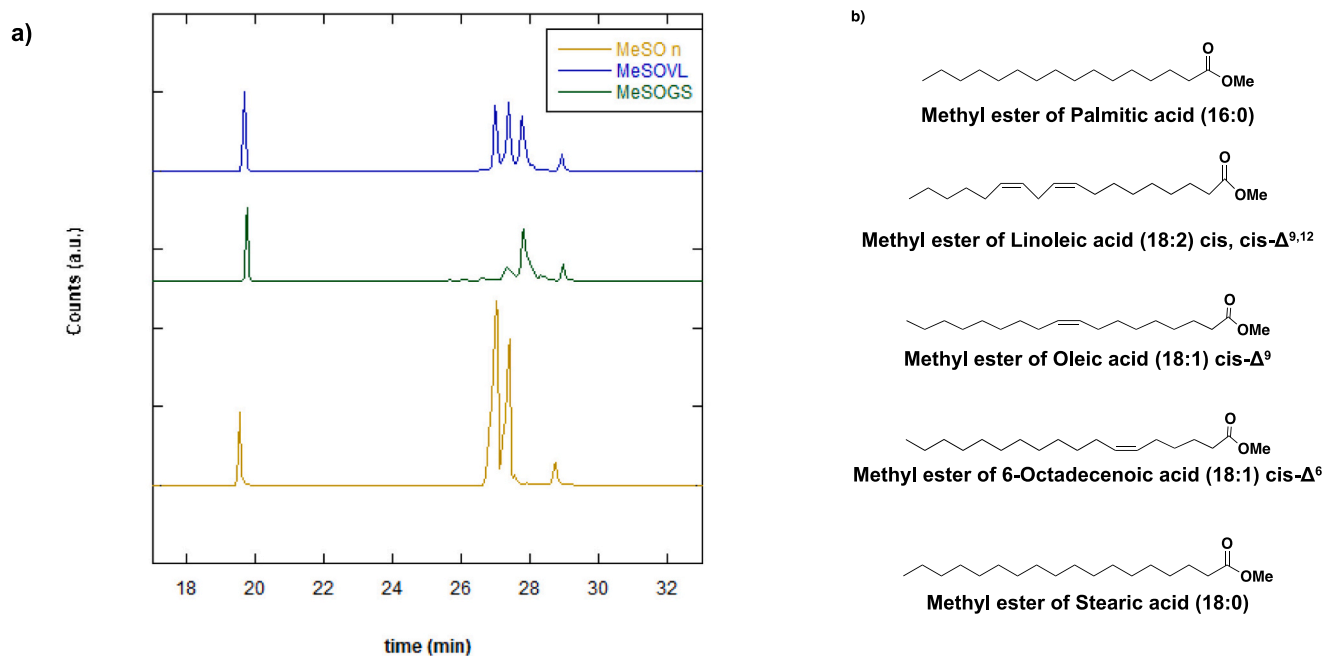


**Fig. 2.** GC chromatograms of SO and SO-derived methyl-esters.

28.8 min, respectively. SO chromatogram, at the bottom of Fig. 2, revealed also the presence of linoleic and oleic acid at retention times of 27.0 and 27.4 min in 55 % and 33 %, respectively (Table 1), confirming the unsaturated fatty acids composition observed by  $^1\text{H}$  NMR analysis. Chromatograms peaks assignment was further assured comparing GC profiles of methyl esters obtained from commercial fatty acids, linoleic and oleic (MeLA, MeOA), used as standards (Fig. S1, Table S1a).

Linoleic acid content decreases in MeSOVL from 55 to 24 % and it is absent in MeSOGS, indicating that linoleic acid reacted overall to obtain the solid. Oleic acid content decreases as well in both MeSOVL and MeSOGS, participating as well in cross-linking reaction. Besides, an isomer of oleic acid, namely 6-Octadecenoic acid (18:1) *cis*- $\Delta^6$ , was also recognized in both polymer forms.

The presence of this isomer with the instauration in position 6 instead of 9 could indicate that an isomerization reaction can occur during the polymer formation. Indeed, the isomerization reaction can favour the formation of Diels-Alder intermediates resulting from the cycloaddition reaction among unsaturated carbons of linoleic and oleic units occurring both inter- and intramolecularly (Scheme 2) [23]. The latter reaction is the origin of the solid material formation.

This isomer of oleic acid, 6-Octadecenoic acid (18:1) *cis*- $\Delta^6$ , is also observed when reaction on olive oil (OO) was performed (Table S1b). However, in that case, only a viscous liquid is obtained without the solid formation. Considering that only 6 % of linoleic acid is present in OO, a large amount of linoleic acid seems crucial to yield the solid.

Thus, the formation of solid material seems mainly governed by the reactivity of linoleic and oleic acid components of SO. This suggestion was proven by reacting both pure acids. In both cases, no solid material formation occurred; hence, triglyceride structures and the nature of unsaturated fatty acids are essential to achieve a solid material formation through cycloaddition and crosslinking (Scheme 1).

### 3.2. Material characterization

#### 3.2.1. ATR-FTIR and X-ray diffraction analysis

More insights regarding the microscopic structure of the SOVL and

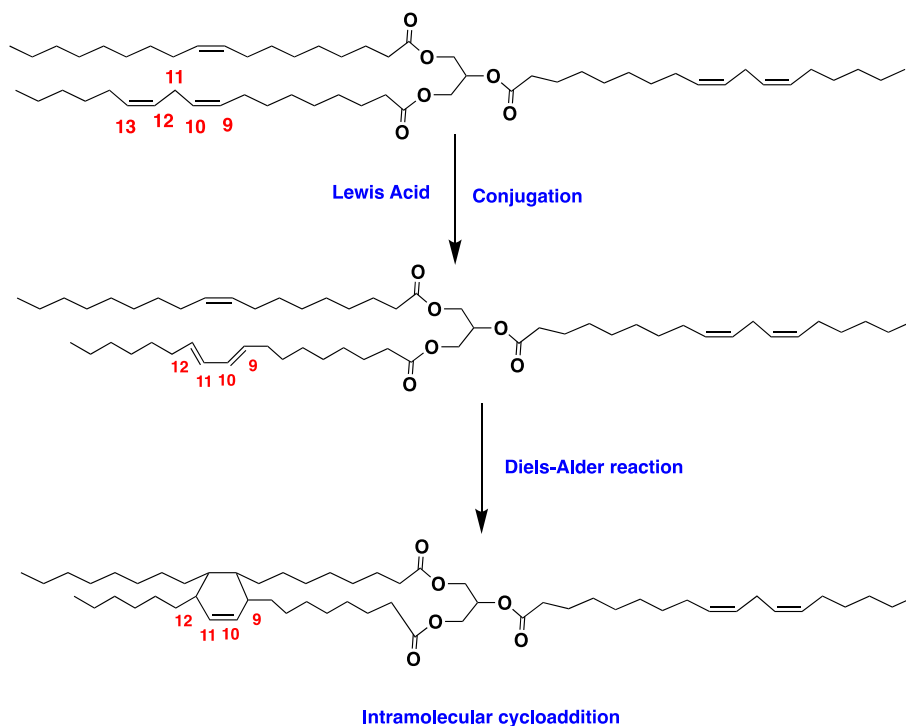
SOGS materials are obtained through Fourier transform infrared spectroscopy in attenuated total reflectance (ATR-FTIR) mode and X-ray diffraction analysis (Fig. 3). The full-band assignment of IR absorbance contributions is reported in Table S2.

Overall, ATR-FTIR spectra of SO, SOVL, and SOGS reveal vibrational modes of  $-\text{CH}_x$ ,  $-\text{O}-\text{C}=\text{O}$ ,  $-\text{CO}$ ,  $-\text{C}=\text{C}$ , and  $-\text{HC}=\text{CH}-$  functional groups (Fig. 3a; Table S2) typically found in vegetable oils and previous reports on other SO derived polymers [24,26]. Yet, the reaction of SO induces significant modifications in IR absorbance of these moieties.

SOVL and SOGS spectra show  $-\text{OH}$  stretching contributions ( $3630\text{--}3430\text{ cm}^{-1}$ ), absent in the SO spectrum, likely deriving from the washing treatment and the subsequent adsorption of water molecules (i. e. air moisture) within both materials. Specifically, the  $-\text{OH}$  band at  $3480\text{ cm}^{-1}$  observed in SOVL relates to intramolecular hydrogen bonding of water to carbonyl groups, which shift towards  $3430\text{ cm}^{-1}$  in the SOGS due to the increased triglyceride local concentration [27]. This ATR-FTIR spectrum also displays a second  $-\text{OH}$  stretching contribution at  $3630\text{ cm}^{-1}$  attributable to less hydrogen-bound water molecules generally observed in heated swollen lipids [28].

The SO reaction substantially changes vibrations of CH from  $\text{HC}=\text{CH}$  bonds at  $3009\text{ cm}^{-1}$ . The latter decreases in intensity, shifts, and splits in two contributions at  $3004$  and a shoulder at  $3009\text{ cm}^{-1}$  in SOVL and disappears in SOGS, confirming the diminished unsaturated fatty acid content observed through GC-MS analysis. The position of this peak links to the unsaturation degree of fatty acids, with  $3009\text{ cm}^{-1}$  attributable to linoleic acid and  $3004\text{ cm}^{-1}$  to oleic acid or 6-Octadecenoic acid [29]. Similarly, the  $-\text{C}=\text{C}$  stretching vibration of *cis*-olefins detected at  $1651\text{ cm}^{-1}$  in the SO spectrum is absent in those of both derivatives. Nevertheless, a peak at  $1640\text{ cm}^{-1}$  arises in SOGS, which derives from  $-\text{OH}$  bending contributions of adsorbed water molecules and  $-\text{C}=\text{C}$  stretching vibrations of carboxyl-sided olefins generally observed for fatty acid thermal mediated-phase transitions [30].

Although all samples display IR contributions related to  $-\text{CH}_x$  stretching modes ( $2960\text{--}2850\text{ cm}^{-1}$ ), the shifting towards shorter wavenumbers observed in the SOGS material for the asymmetric ( $2920\text{ cm}^{-1}$ ) and symmetric ( $2851\text{ cm}^{-1}$ )  $-\text{CH}_2$  vibrations indicate that the



**Scheme 2.** Schematic representation of possible Diels-Alder intermediate resulting from the cycloaddition reaction among unsaturated carbons of linoleic and oleic units. It is shown only the intramolecular attack for clarity [23].

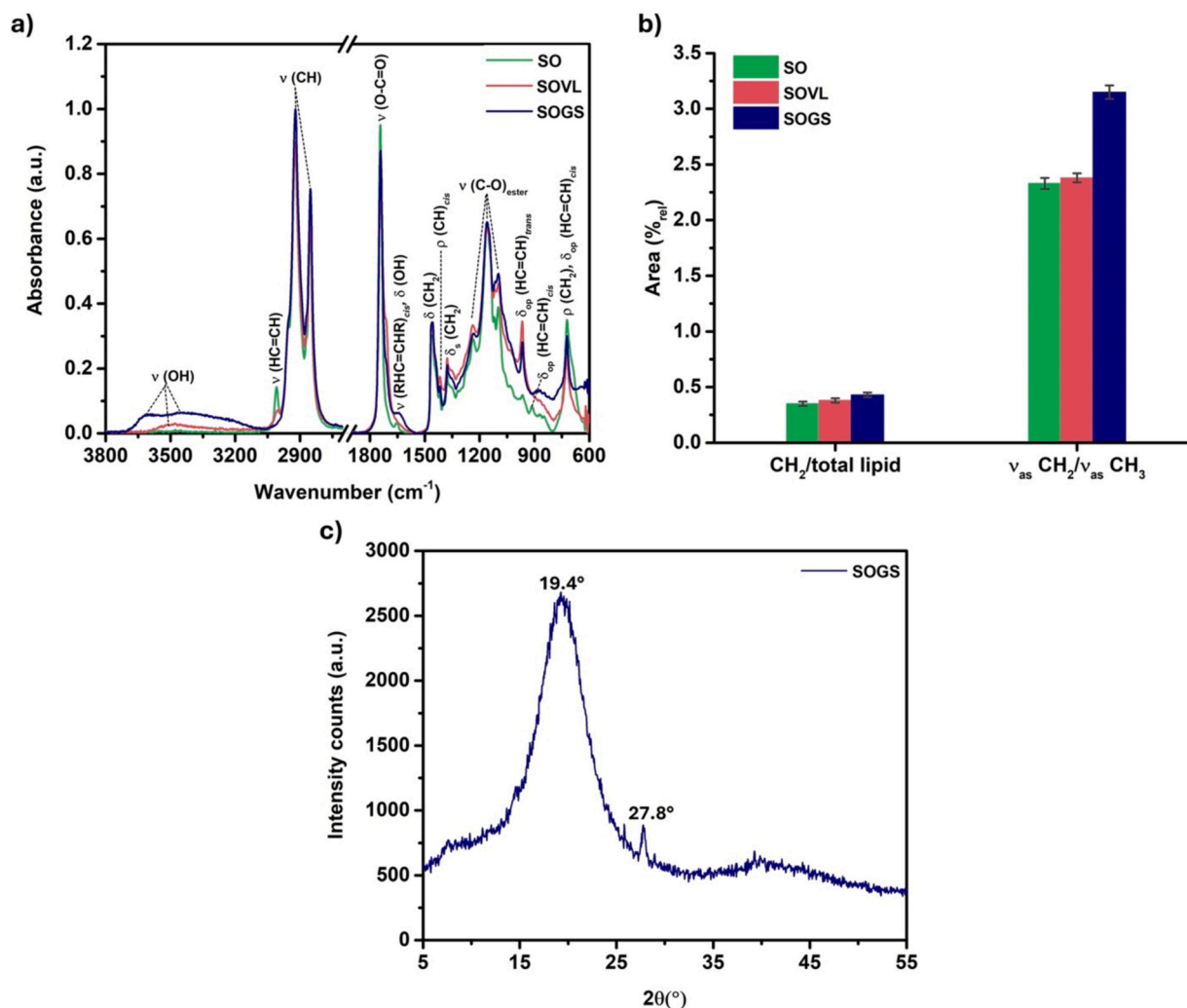


**Fig. 3.** (a) ATR-FTIR spectra of SO and the derived polymers, (b) normalized integrals and ratios of relevant and diagnostic IR modes referring to the acyl chains of fatty acids, and (c) XRD pattern of SOGS.

reaction led to ordered and more saturated, hence more rigid, acyl chains [31,32]. This outcome is further corroborated by spectral deconvolutions in the 3000–2800 cm<sup>-1</sup> region (Fig. S2; Table S3), which also highlights an increased -CH<sub>2</sub>-to-total lipid integrals, typical of saturated lipids, and peak area ratio of the asymmetric -CH<sub>2</sub>-to-asymmetric -CH<sub>3</sub> contributions (Fig. 3b) [31,32]. Modifications occurring within the acyl chains of triglycerides due to SO reaction are also visible by the variations of the -CH<sub>2</sub> wagging vibrational modes. In this regard, peaks at 1319, 1059, and 847 cm<sup>-1</sup> of the SO spectrum disappear, shift, or are reduced in the derivatives, being more evident for the SOGS than SOVL and a new shoulder simultaneously appears at ca. 1340 cm<sup>-1</sup>, which is typical of the same vibrational mode but for end gauche conformers [33].

The SO reaction also causes the disappearance of the -CH bending (1398 cm<sup>-1</sup>) and the out-of-plane -HC=CH- bending (914 cm<sup>-1</sup>) vibrations related to *cis*-olefinic groups and *cis*-double bonds in SOVL and SOGS [29,34]. This evidence, alongside the increased absorption of -CH bending of double bonds in *trans* configuration at 967 cm<sup>-1</sup> detected for both materials [29,34], may suggest a rearrangement of *cis* in *trans* double bonds within SO [35] induced by Lewis Acids, which can favour the cross-linking reaction through a Diels-Alder adduct.

On the other hand, all samples feature IR absorbance related to -O-C=O stretching (ca. 1740 cm<sup>-1</sup>) vibration diagnostic for the ester bond, indicating the maintenance of this moiety even after the reaction. Yet, both derivatives display a secondary broad -O-C=O stretching

contribution at lower wavenumbers attributed to free fatty acids. The two -O-C=O contributions at ca 1740 and 1710 cm<sup>-1</sup> refer to the hydrophobic carbonyl of the *sn*-1 acyl chain or the carbonyl group of the *sn*-2 acyl chain close to the polar head region, respectively [27]. The low wavenumber-vibrational mode arises in both synthesized materials due to the formation of intramolecular hydrogen bonds [27], as indicated by the broadness of this band and the detection of -OH stretching contributions. Besides, the small shift and decreased intensity observed in SOGS than SOVL can link to the heating procedure and the variation from liquid to solid state of the material itself. Indeed, high temperatures disrupt hydrogen bonds [27].

Variations regarding the -COO portion of SO triglycerides are further confirmed by the disappearance of the O-C=O bending vibration (687 cm<sup>-1</sup>), the appearance of the -CO stretching mode at ca. 1300 cm<sup>-1</sup>, and the shift of -C-O-, -C-O-C, and =C-O-C stretching contributions in the 1140–1030 cm<sup>-1</sup> region in both materials. These modifications are consistent with the heating procedure [35].

The SOGS is further characterized through XRD analysis (Fig. 3c) to evaluate its crystalline structure and degree of crystallinity (DC), parameters that significantly influence materials' physical-chemical and technological properties. The XRD pattern shows an amorphous scattering halo typical of a semicrystalline polymer with low crystallinity [36], as also confirmed by the calculated DC of 32%. In line with previous reports on SO-derived polymers [37–39], SOGS also displays a broad diffraction peak at 19.4° and a secondary low-intensity signal at

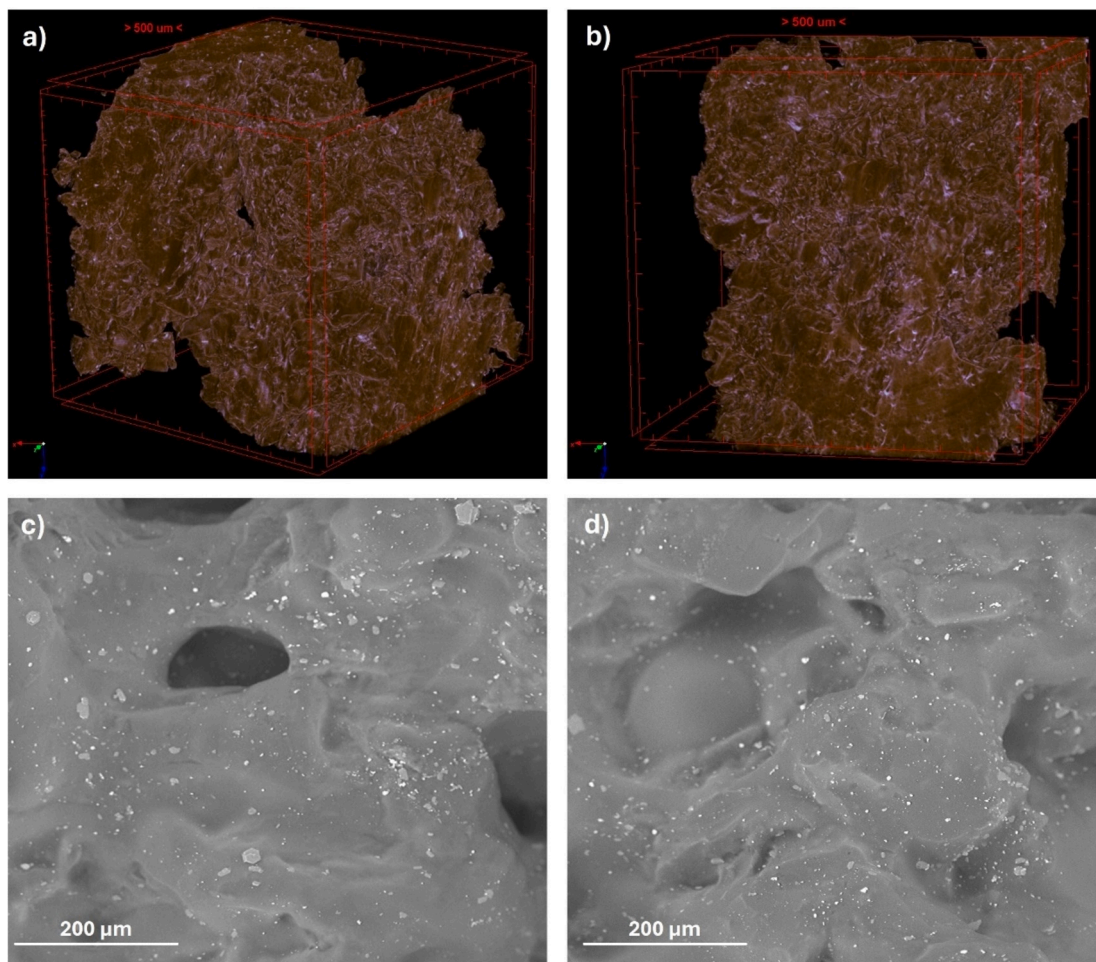


Fig. 4. (a-b) Nanotomography and (c-d) SEM imaging of SOGS in different areas.

27.8°. These diffraction peaks are similar to those of polyvinyl alcohol and polyvinyl chloride polymers, inferring the potential formation of fringed micellar microcrystals [40,41] during the SO reaction. Specifically, the high intensity of the 19.4° peak, typical of amorphous polymers [37], likely derives from the thick and heterogeneous network structure of SOGS, which in turn infers on a high degree of polymer aggregation [42].

### 3.2.2. Morphology of bio-based material through SEM and nanotomography analysis

The SOGS morphology was evaluated through nanotomography and SEM imaging in different areas of the material (Fig. 4) to verify its homogeneity. Moreover, elemental analysis was performed (Fig. S3) to evaluate its composition and the potential presence of residual contaminants deriving from the reaction procedure.

Nanotomography sections and SEM images show that SOGS is overall homogeneous, yet some macroaggregates and cavities are visible on its surface, which becomes uneven.

This outcome derives from the heating procedure, which favors the loss of the liquid component and the solid aggregation, whose rate and extent are not easily controllable, aligning with XRD analysis. The elemental analysis performed through energy-dispersive X-ray spectroscopy (EDX) indicates carbon and oxygen as the main components of SOGS.

### 3.2.3. Thermal properties of bio-based material

DSC analysis of SOGS shows a glass transition at 84 °C (Fig. 5), while the material was not degraded until 300 °C, thus indicating a possible

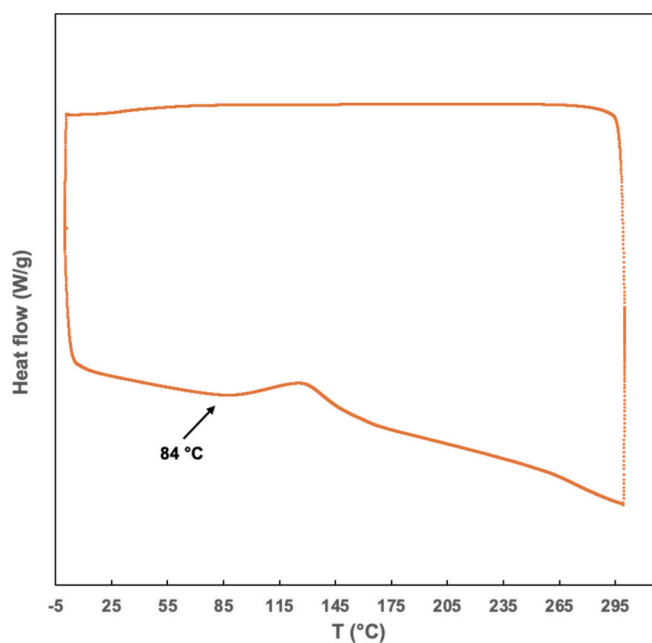


Fig. 5. DSC trace of SOGS. Heat flow Exothermic peaks point upward.

use of the material also at high temperatures in line with similar thermoset polymers [6].

Considering that SO is liquid and does not show any thermal transition, the glass transition at 84 °C observed for SOGS indicates a good degree of crosslinking ability of the material in line with the thermal behaviour of some ESO crosslinked polymers [4,13].

### 3.2.4. Swelling ability

The presence of several cavities observed by SEM and nanotomography analysis, led to test the swelling ability (Q) of the solid in several solvents (Fig. S4). Q was calculated as previously reported [43] and according to Eq. (1).

The swelling ability was negligible in acetonitrile, acetone, methanol and hexane, indicating the high resistance of the materials to the adsorption of these solvents and confirming the low porosity observed by nanotomography analysis. This trend can also be indicative of a good crosslinking ability, conferred also by a low content of double bonds in the structure as previously observed for some epoxidized SO copolymer derivatives [12]. On the other hand, SOGS showed the highest Q in  $\text{CHCl}_3$  and THF, with values of 15 and 8, respectively (Fig. 6 and Table S4). In dependence of the solvent used an increase in swelling ability was then observed, for this reason the good adsorption ability of  $\text{CHCl}_3$  encouraged to test the adsorption ability of this halogenated solvent from wastewater.

### 3.3. Bio-based materials as adsorbent for wastewater pollutants

So far, several adsorbents have been used for wastewater remediation [19,44–47]. The use of bio-based materials as adsorbents for wastewater pollutants have been encouraged thanks to their higher porosity, surface area and processing nevertheless thanks to the potential non-toxicity of the adsorbent. For this reason, pure biopolymer or most commonly composite materials have been tested for recovery of oil-spill from saline solutions [48], dyes, heavy metals [49] or other contaminants [50]. This finding opens a new path for the development of new, high efficiency, ecologically acceptable, and cheaper dispersant for wastewater remediation.

#### 3.3.1. Adsorption of halogenated solvents from wastewater

To test the adsorption efficiency of SOGS, a certain amount of material was placed in contact with a  $\text{CHCl}_3$  saturated solution in water (8 mg/mL). The amount of residual  $\text{CHCl}_3$  in water was determined via SPME-GC-MS through a calibration curve [51] and the efficiency (E %) was calculated according to Eq. 2. Results are reported in Fig. 7 and Table S5.

## Adsorption of Chloroform from wastewater

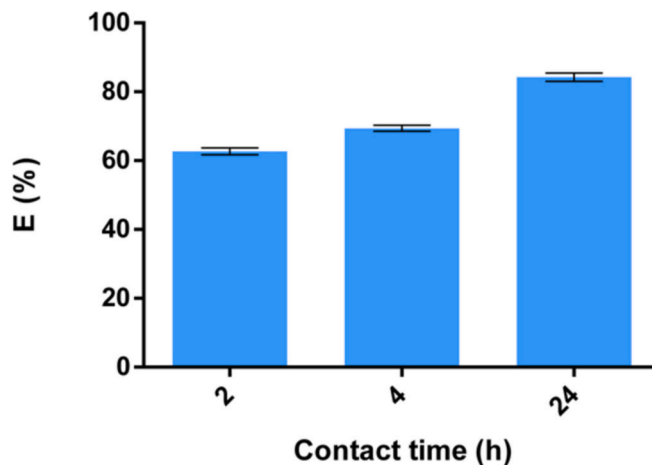


Fig. 7. Efficiency of SOGS adsorption of  $\text{CHCl}_3$  from aqueous solution (8 mg/mL) at different contact times at room temperature. E % is based on triplicate runs.

After 2 h of contact, we immediately observed an efficiency of 62 %, which increases up to 83 % in 24 h confirming the high swelling ability of SOGS in  $\text{CHCl}_3$ . So far, only few examples of polymer materials used for the adsorption of toxic halogenated solvent have been reported, such as some ZnO polymers sponges [52]. Data of adsorption tests are not directly comparable with the one obtained using SOGS as an adsorbent, as the  $\text{CHCl}_3$  adsorption values of the former have been calculated in terms of swelling of pure halogenated solvent and not in water solution.

#### 3.3.2. Adsorption of organic dyes from wastewater

Other organic molecules can be responsible for wastewater, for this reason adsorption efficiency of SOGS was tested in different dye water solutions used as model pollutants (Table S6). SOGS showed the best adsorption efficiency (E, calculated as a percentage value) for the cationic dye Rhodamine B (RhB), whose adsorption process was further studied. Selectivity for cationic or anionic dyes has been observed also as a function of the different functionalization of some chitosan-based polymers [53].

UV–visible spectra of the RhB solution after being in contact with SOGS at different times reveal a decreased absorbance with a maximum at 554 nm at longer contact times with SOGS, corresponding to a less

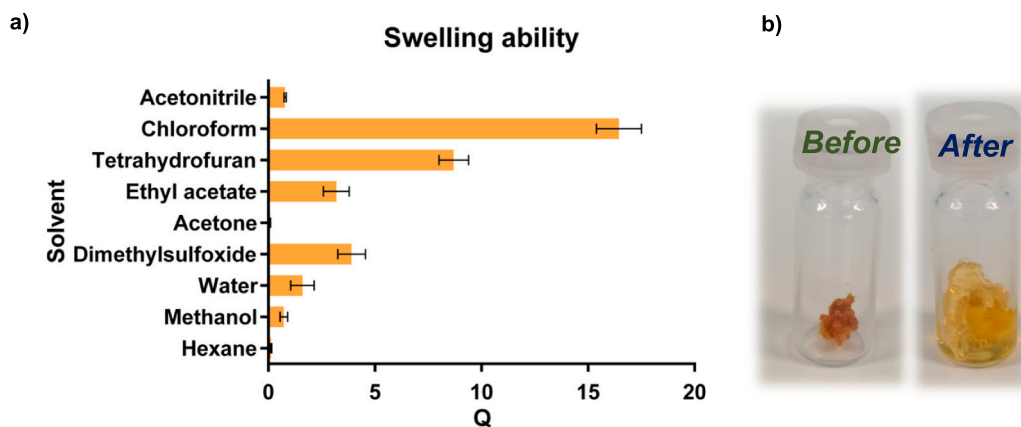
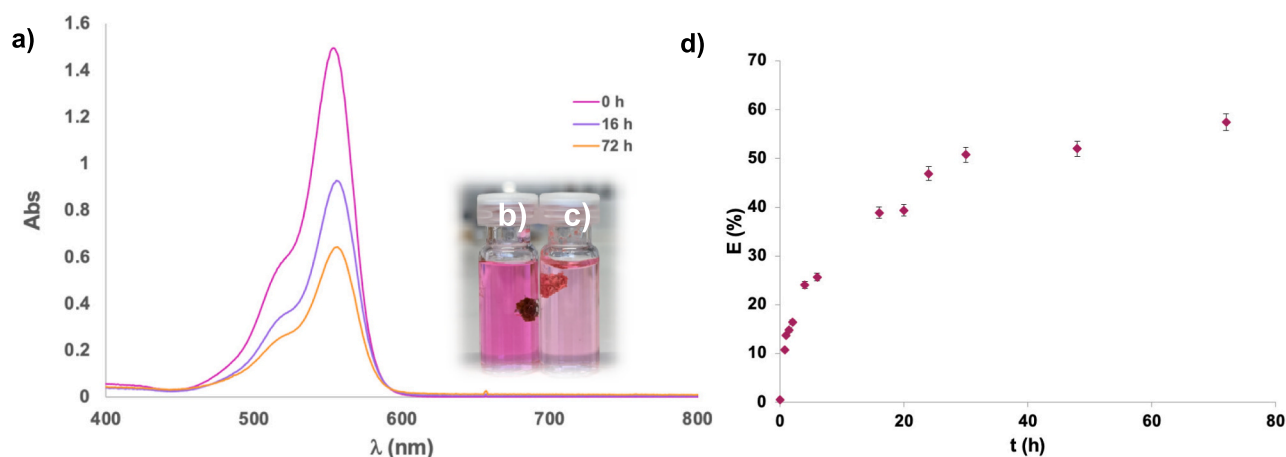
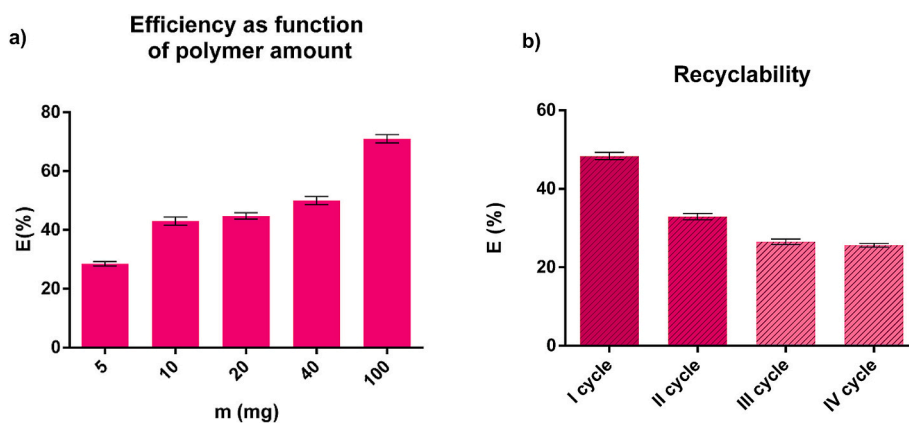


Fig. 6. Histogram reporting values of swelling ability (Q) of SOGS in a) different solvents and b) picture of SOGS before and after swelling in THF. Q is based on triplicate runs.



**Fig. 8.** a) UV-vis spectra of RhB water solution at different contact times with SOGS; picture of SOGS in contact with RhB solution at time b) 0 h and c) 24 h; d) kinetic of efficiency (E) of SOGS adsorption of RhB from aqueous solution ( $1.8 \times 10^{-5}$  M) at different contact times at room temperature. E % is based on triplicate runs.



**Fig. 9.** Adsorption efficiency of RhB ( $1.8 \times 10^{-5}$  M) as function of SOGS at room temperature in 24 h. E % is based on triplicate runs.

coloured solution (Fig. 8b-c).

Adsorption kinetic of RhB water solution in presence of SOGS has been carried out evaluating the % efficiency (E) according to Eq. 2. The adsorption of RhB gradually increases until reaching a plateau at 24 h with E of 45 % (Fig. 8d). This value slightly increases up to 57 % in 72 h. Some acrylated epoxidized soybean oil used as adsorbent for methylene blue dye, showed a similar removal efficiency as less than 70 % was reached and they need to add graphene oxide and chitosan to enhance dye adsorption efficiencies [54].

The use of SOGS can guarantee an easy handling of the adsorbent from wastewater solution. For this reason, an investigation on the effect of the amount of SOGS at 24 h of contact with RhB solution was performed (Fig. 9a).

As expected, E % increases as a function of the amount of SOGS, with the highest value obtained using 100 mg of SOGS (Fig. 9a), even though the variation is not significant from 10 to 40 mg of material (Table S7). Hence, 20 mg of SOGS can be used as the average amount needed for good adsorption of RhB.

Finally, the recycling ability of SOGS was evaluated after the desorption of RhB from the material (Fig. S5). Desorption process of dyed-SOGS was performed using bio-based solvents such as 2-MeTHF and EtOH, that can replace petroleum-based solvents having less environmental consequence [55]. Both solvents warranted great desorption ability, as RhB was totally desorbed after immersing the dyed-SOGS in the proper solvent for 3 cycles of 15 min and ultrasound irradiation. Nevertheless, recovered SOGS using 2-MeTHF assures good E % differently from the one recovered using EtOH that registered a drop in

efficiency already at the first cycle after adsorption of the fresh dye solution.

E % slightly decreases in the recycled SOGS and it could be effectively employed for nearly 4 cycles, this indicates that the material, possesses moderate recycling ability as previously observed for other systems [54] and can be recycled up to 4 cycles with good E% (Fig. 9b, Table S8).

### 3.4. Chemical degradation of SOGS

Testing the end-of-life of materials is also a crucial step, in addition to the selection of valuable bio-source and the use of a greener synthetic approach to obtain new bio-based materials [56,57]. Indeed, converting bio-based feedstock in polymers is challenging and beneficial to reduce environmental pollution, but it should be supported by the degradability of the bio-based material, as several new biopolymers do not meet this last criterium contributing to increasing the presence of solid wastes in the environment.

For this reason, chemical degradability of SOGS has been tested in several solvents and using different quantities of bases or acids. SOGS degradation was tested immersing it in bases such as NaOH or KOH in methanol and in water and in an acidic water solution of HCl. The percentage of chemical degradation (D) was calculated according to Eq. 3 (Table S9). Fig. 10 shows how SOGS is degraded in basic conditions rather than in acidic ones (Fig. 10c).

In the water solution of KOH (2 M) the presence of emulsion liquids with no residual SOGS formed was observed (Fig. 10a), in agreement



Fig. 10. Pictures of SOGS before and after degradation treatment in different experimental conditions.

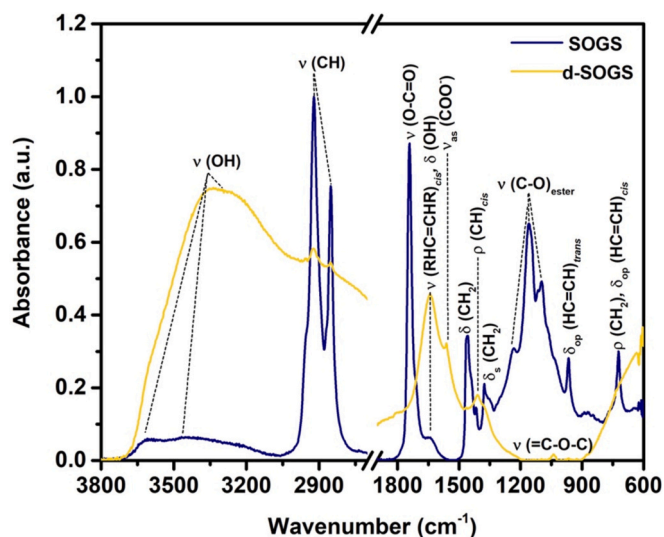


Fig. 11. ATR-FTIR spectra of SOGS and d-SOGS.

with previously reported literature [10]. These showed that there was complete degradation under aqueous KOH (chemical degradation = 97 %, Table S9). While the presence of a less strong base, NaOH (2 M), gives a 47 % of chemical degradation and the presence of both liquid emulsion and some residual SOGS can be observed. On the other hand, the use of lower quantity of NaOH (1 wt%) in methanolic solution favored the complete degradation.

These data suggest the hydrolytic cleavage of ester bonds as expected [10], which was evaluated by performing ATR-FTIR spectroscopy on the degraded solid (d-SOGS) (Fig. 11, Table S10).

The degradation of d-SOGS was confirmed by its ATR-FTIR spectrum, which features less vibrational modes than SOGS. Specifically, IR contributions related to carbonyl groups, either in *sp*-1 or *sp*-2 conformations, disappeared in d-SOGS, aligning with the hypothesis of a hydrolytic cleavage of ester bonds. The latter is also corroborated by the arising of a signal at ca.  $1561\text{ cm}^{-1}$ , which is typical of the asymmetric  $\text{-COO}^-$  stretching vibration of potassium salts of linoleic and oleic acids [58,59], and the decreased and shifted  $\text{-CH}_x$  stretching modes ( $2960\text{--}2850\text{ cm}^{-1}$ ) related to fluid and disordered acyl chains [31,32]. Lastly, the increased intensity of  $\text{-OH}$  stretching ( $3340\text{ cm}^{-1}$ ) and bending ( $1642\text{ cm}^{-1}$ ) derive from the KOH water solution used for degrading SOGS.

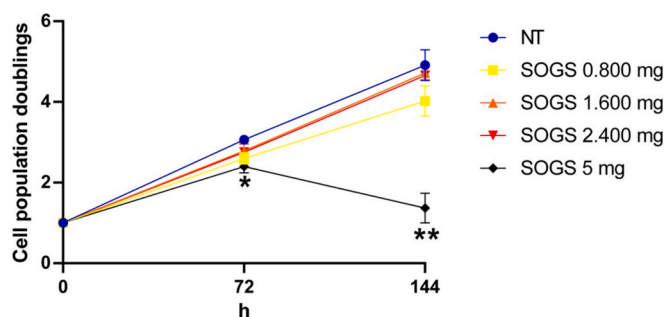


Fig. 12. Evaluation of SOGS effect on the proliferation of RPE-1 cells. Graph showing the number of doublings that the RPE-1 cell population has undergone since the treatment with the indicated amounts of SOGS and up to 6 days (144 h). Untreated cells are used as control (NT). The final volume of all the samples suspension is 1 mL. Graph represents the mean  $\pm$  SEM of at least three independent experiments. Un-paired *t*-test between the NT sample and the different treatments: \*  $p < 0.05$ , \*\*  $p < 0.01$ .

### 3.5. Biocompatibility of the bio-based material, the *in vitro* cytotoxicity and cell viability assays

The effect of SOGS on the viability of normal cells was tested on the

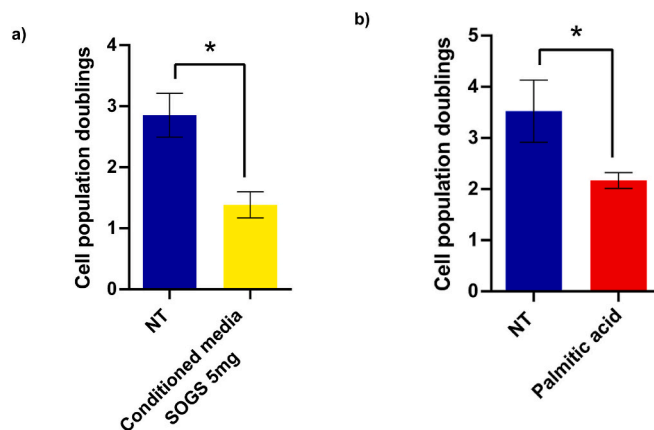


Fig. 13. Evaluation of the effects due to SOGS released-components on the proliferation of RPE-1 cells. Histograms showing the number of doublings that the RPE-1 cell population has undergone after 72 h since the treatment with conditioned media recovered from 5 mg SOGS incubation for 3 days (a), or with 1 mg palmitic acid (b). Untreated cells are used as control (NT). The final volume of all the samples suspension is 1 mL. Graphs summarize the mean  $\pm$  SEM of three independent experiments. Un-paired *t*-test between the NT sample and the different treatments: \*  $p < 0.05$ .

normal, non-tumoral human retinal pigment epithelial cell line RPE-1. Cell proliferation analysis was performed for 6 days (144 h) of treatment with different amounts of SOGS. Considering that SOGS is insoluble in aqueous solutions, we weighted the indicated amount of material and directly placed it into the culture media. Material-free culture media was used as a control (NT). Results showed that SOGS did not affect the proliferation of RPE-1 cells in three of the tested amounts (0.8 mg, 1.6 mg and 2.4 mg in 1 mL culture media) (Fig. 12). Only the highest tested concentration of SOGS (5 mg in 1 mL) significantly affected cell proliferation, especially in longer treatments (144 h).

We reasoned that the high concentration of SOGS could release something in the solution that could affect cell proliferation. Hence, we let the cells grow in a conditioned media derived from culture media left in the presence of 5 mg SOGS for 3 days which contains all the components eventually released by the material. We collected the conditioned media after 3 days of incubation, as at this time 5 mg SOGS already affected the proliferation of RPE-1 cells (Fig. 12). We grew RPE-1 cells in the conditioned media for 3 days and observed a similar reduction in cell proliferation as upon incubation with 5 mg SOGS (Fig. 12 and 13a), suggesting that this amount of SOGS releases a component in the culture media that affects cell proliferation. Since SOGS could release fatty acids, we tested the effect of palmitic acid (1 mg/mL) on the proliferation of RPE-1 cells. The results illustrated in Fig. 13b showed that palmitic acid induced a slowing-down of RPE-1 cells proliferation comparable to that induced by 5 mg SOGS.

Finally, we tested the metabolic activity of RPE-1 cells, and thus their cell viability, by MTT (3-[4,5-dimethylthiazol-2-yl]-2,5 diphenyl tetrazolium bromide) assay, under treatment with different amounts of SOGS for 24 h. The obtained results showed that none of the tested concentrations (0.8 mg, 1.6 mg and 2.4 mg in 200  $\mu$ L culture media) arrested the metabolic activity of RPE-1 cells (Fig. 14). In addition, it is possible to notice that the half-maximal inhibitory concentration  $IC_{50}$  was not reached even with the highest amount of SOGS tested.

Collectively, these results showed that the cells were able to proliferate and survive till the end of the treatment (6 days), suggesting that SOGS is not toxic for normal cells (Fig. 12). Similarly, the MTT assay revealed that five times increased concentrations of SOGS (0.8 mg/200  $\mu$ L – 2.4 mg/200  $\mu$ L) only slightly impact cell metabolic activity after 24 h of treatment (Fig. 14). This maximum concentration is comparable to the one used for adsorption tests (13 mg/mL). Importantly,  $IC_{50}$  was not reached with these concentrations, excluding a cytotoxic effect of aSOGS. We only observed a reduction of the cell proliferation, though without cell death, when using the 5 mg/mL SOGS concentration (Fig. 12). It is important to mention that, considering the insolubility of SOGS in aqueous solution, as the culture media is, the solid remains floating on the culture media in the well with the cultured cells. However, something released in solution could disturb cell proliferation. Indeed, when RPE-1 cells were treated for 3 days with a conditioned media (previously incubated with 5 mg SOGS for 3 days) the impact on cell proliferation was similar to that obtained in the presence of the compound at the same timepoint (Fig. 13a). Hypothesizing that fatty acids released by SOGS could induce this effect, we tested the biocompatibility of palmitic acid (1 mg/mL), whose antiproliferative effect results to be even slightly higher than the SOGS itself (Fig. 13b). Palmitic acid is the most common circulating saturated fatty acids (approximately 28 % of normal human plasma lipid content) [60]; however, at high doses generally induces cellular dysfunctions [61]. This suggests that SOGS has a less cytotoxic effect compared to this common organic compound supporting the idea of its safe usage in the environment.

#### 4. Conclusions

A greener synthetic approach to obtain simply SO-derived materials has been proposed. The use of microwaves and a smaller amount of catalyst allow to decrease the overall impact of the synthetic pathway. Fresh or expired SO has been used as starting material without further

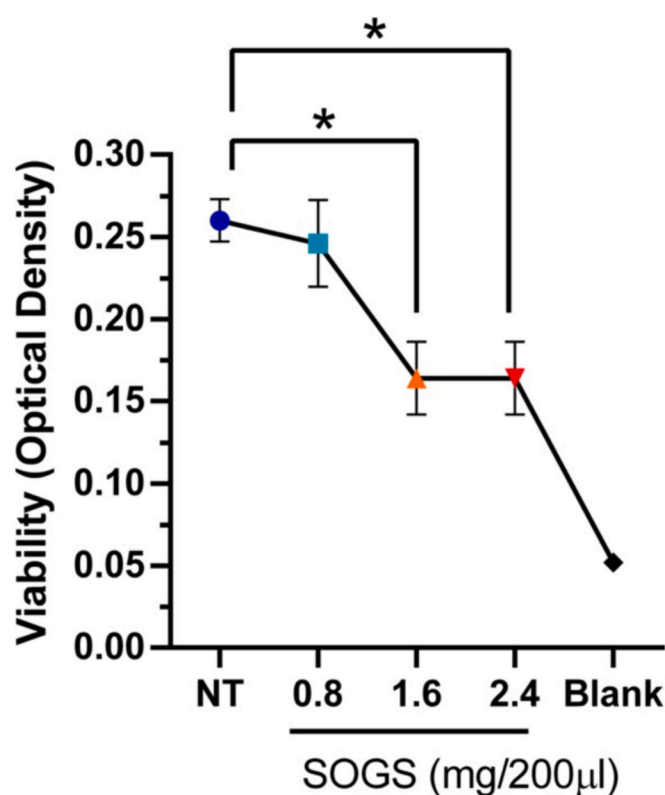


Fig. 14. RPE-1 cell viability measured using the MTT assay under SOGS exposure. Graph showing the optical density (OD), as a function of cell metabolic activity and thus of cell viability, of RPE-1 cells treated or not with SOGS at the indicated concentrations. Absorbance was measured following 24 h of incubating cells with SOGS. Data are shown as mean OD of triplicate wells and error bars represent the SEM. Un-paired t-test between the NT sample and the different treatments: \*  $p < 0.05$ .

chemical modifications.

The synthesis of the material occurs through the reactivity of unsaturated fatty acid chains forming the SO triglycerides structures, as confirmed by  $^1H$  NMR, GC-MS and ATR-FTIR analysis. The presence of some isomeric form of oleic acids probably also indicates the formation of a Diels-Alder adduct favoring the cross-linking reaction as previously observed.

Bio-based material showed a compact morphology with few cavities that allow, in the presence of some solvents, a good swelling ability, while in most of the solvents, the material showed a good resistance. SOGS revealed a glass transition at 84  $^{\circ}C$  and thermal stability up to 300  $^{\circ}C$ . SOGS can also be chemically degraded in water under basic conditions, and it is biocompatible, according to biological tests on normal cells.

A preliminary investigation of SOGS as an adsorbent material for wastewater treatment was performed by evaluating its adsorption ability for  $CHCl_3$  and dyes, showing good adsorption efficiencies and recycling ability, opening the use of this material also for the adsorption of emerging pollutants, as few example are so far reported [19].

Biological tests confirmed that this material is biocompatible. Hence, it can be used to develop innovative technologies to transform natural resources into smart multifunctional materials for a wide range of applications, including adsorbent for environmental remediation, coatings, adhesives, and medical devices.

#### Funding

Carla Rizzo thanks PNR next generation EU-DM737/2021-CUP B79J21038330001 and PJ\_UTILE\_2022\_VQR\_Misura\_B\_D15\_Rizzo

granted by Università degli Studi di Palermo for funding.

### CRedit authorship contribution statement

**Viviana Barra:** Data curation, Writing – original draft. **Elena Piazenza:** Data curation, Writing – original draft. **Sara Amata:** Investigation, Data curation. **Salvatore Martino:** Investigation. **Filippo Vitale:** Investigation. **Delia Francesca Chillura Martino:** Validation. **Silvestre Buscemi:** Visualization. **Carla Rizzo:** Writing – original draft, Methodology, Funding acquisition, Conceptualization, Writing – review & editing. **Antonio Palumbo Piccionello:** Writing – review & editing, Supervision, Methodology, Conceptualization.

### Declaration of competing interest

None.

### Acknowledgements

This work was supported by the Italian Ministry of Education, University, and Research (MUR) through the National Operational Programme (PON) Project on Research and Innovation 2014-2020 (Azione IV.v – Contratti di ricerca su tematiche dell'Innovazione – B75F21002190001). We thank AtenCenter at the University of Palermo for SEM and tomography experiments.

### Appendix B. Supplementary data

GC chromatograms of LA and OA methyl esters, deconvolutions of ATR-FTIR spectra, EDX spectra, swelling and desorption tests pictures. Tables of methyl esters analysis of OO reaction, ATR-FTIR absorption contributions, vibrational modes and parameters obtained from deconvolutions of ATR-FTIR spectra, swelling ability of SOGS in different solvents, adsorption Efficiency of Chloroform from wastewater, adsorption Efficiency of different dyes from wastewater, RhB adsorption efficiency as function of material amount, RhB adsorption efficiency after recyclability SOGS, percentage of chemical degradation ability, ATR-FTIR absorption contributions of SOGS and d-SOGS and their identification. Supplementary data to this article can be found online at [<https://doi.org/10.1016/j.susmat.2024.e01216>].

### Data availability

Data will be made available on request.

### References

- [1] S.K. Kumaran, M. Chopra, E. Oh, H.-J. Choi, Chapter 11 - Biopolymers and natural polymers, in: R. Narain (Ed.), *Polymer Science and Nanotechnology*, Elsevier, 2020, pp. 245–256, <https://doi.org/10.1016/B978-0-12-816806-6.00011-X>.
- [2] N. Hernández, R.C. Williams, E.W. Cochran, The battle for the “green” polymer. Different approaches for biopolymer synthesis: bioadvantaged vs. bioreplacement, *Org. Biomol. Chem.* 12 (18) (2014) 2834–2849, <https://doi.org/10.1039/C3OB42339E>.
- [3] D.D. Andjelkovic, R.C. Larock, Novel rubbers from cationic copolymerization of soybean oils and dicyclopentadiene. 1. Synthesis and characterization, *Biomacromolecules* 7 (3) (2006) 927–936, <https://doi.org/10.1021/bm050787r>.
- [4] Z. Qian, S. Liu, G. Du, S. Wang, Y. Shen, X. Zhou, S. Jiang, H. Niu, Z. Duan, T. Li, Versatile epoxidized soybean oil-based resin with excellent adhesion and film-forming property, *ACS Sustain. Chem. Eng.* 11 (13) (2023) 5315–5324, <https://doi.org/10.1021/acssuschemeng.3c00743>.
- [5] Y. Xia, R.C. Larock, Vegetable oil-based polymeric materials: synthesis, properties, and applications, *Green Chem.* 12 (11) (2010) 1893–1909, <https://doi.org/10.1039/C0GC00264J>.
- [6] F. Li, R.C. Larock, Novel polymeric materials from biological oils, *J. Polym. Environ.* 10 (1) (2002) 59–67, <https://doi.org/10.1023/A:102106224642>.
- [7] X.-L. Wang, L. Chen, J.-N. Wu, T. Fu, Y.-Z. Wang, Flame-retardant pressure-sensitive adhesives derived from epoxidized soybean oil and phosphorus-containing dicarboxylic acids, *ACS Sustain. Chem. Eng.* 5 (4) (2017) 3353–3361, <https://doi.org/10.1021/acssuschemeng.6b03201>.
- [8] Y. Chen, Y. Zeng, Y. Wu, T. Chen, R. Qiu, W. Liu, Flame-retardant and recyclable soybean oil-based thermosets enabled by the dynamic phosphate ester and tannic

- acid, *ACS Appl. Mater. Interfaces* 15 (4) (2023) 5963–5973, <https://doi.org/10.1021/acsmi.2c21279>.
- [9] Y. Wu, M. Fei, T. Chen, R. Qiu, W. Liu, Fabrication of degradable and high glass-transition temperature thermosets from palm oil and isosorbide for fiber-reinforced composites, *Ind. Crop. Prod.* 170 (2021) 113744, <https://doi.org/10.1016/j.indcrop.2021.113744>.
- [10] W. Li, Q. Zhan, P. Yang, Facile approach for the synthesis of performance-advantaged degradable bio-based thermoset via ring-opening metathesis polymerization from epoxidized soybean oil, *ACS Sustain. Chem. Eng.* 11 (3) (2023) 1200–1206, <https://doi.org/10.1021/acssuschemeng.2c06787>.
- [11] S.N.H. Mustapha, A.R. Rahmat, A. Arsad, Bio-based thermoset nanocomposite derived from vegetable oil: a short review 30 (2) (2014) 167–182, <https://doi.org/10.1515/revce-2013-0010>.
- [12] Q. Wu, Y. Hu, J. Tang, J. Zhang, C. Wang, Q. Shang, G. Feng, C. Liu, Y. Zhou, W. Lei, High-performance soybean-oil-based epoxy acrylate resins: “green” synthesis and application in UV-curable coatings, *ACS Sustain. Chem. Eng.* 6 (7) (2018) 8340–8349, <https://doi.org/10.1021/acssuschemeng.8b00388>.
- [13] S.A. Madbouly, S. Yamane, A.J.V.D. Vlies, U. Hasegawa, Biobased semi-interpenetrating polymer networks of poly( $\epsilon$ -caprolactone) and epoxidized soybean oil with nanoscale morphology, shape-memory effect, and biocompatibility, *ACS Appl. Polymer Mater.* 5 (11) (2023) 8907–8918, <https://doi.org/10.1021/acsp.3c01270>.
- [14] T.A. Fernandes, I.F.M. Costa, P. Jorge, A.C. Sousa, V. André, R.G. Cabral, N. Cerca, A.M. Kirillov, Hybrid silver(I)-doped soybean oil and potato starch biopolymer films to combat bacterial biofilms, *ACS Appl. Mater. Interfaces* 14 (22) (2022) 25104–25114, <https://doi.org/10.1021/acsmi.2c03010>.
- [15] S. Zhou, K. Huang, X. Xu, B. Wang, W. Zhang, Y. Su, K. Hu, C. Zhang, J. Zhu, G. Weng, S. Ma, Rigid-and-flexible, degradable, fully biobased thermosets from lignin and soybean oil: synthesis and properties, *ACS Sustain. Chem. Eng.* 11 (8) (2023) 3466–3473, <https://doi.org/10.1021/acssuschemeng.2c06990>.
- [16] S. Roy Goswami, S. Sudhakaran Nair, X. Zhang, N. Tanguy, N. Yan, Starch maleate/epoxidized soybean oil/poly(lactic acid) films with improved ductility and biodegradation potential for packaging fatty foods, *ACS Sustain. Chem. Eng.* 10 (43) (2022) 14185–14194, <https://doi.org/10.1021/acssuschemeng.2c03881>.
- [17] M. Zubair, A. Ullah, Chapter 14 - Biopolymers in environmental applications: Industrial wastewater treatment, in: S. Thomas, S. Gopi, A. Amalraj (Eds.), *Biopolymers and their Industrial Applications*, Elsevier, 2021, pp. 331–349, <https://doi.org/10.1016/B978-0-12-819240-5.00014-6>.
- [18] P.R. Yaashikaa, P. Senthil Kumar, S. Karishma, Review on biopolymers and composites – Evolving material as adsorbents in removal of environmental pollutants, *Environ. Res.* 212 (2022) 113114, <https://doi.org/10.1016/j.envres.2022.113114>.
- [19] H. Sreehari, V. Gopika, J.S. Jayan, A.S. Sethulekshmi, A. Saritha, A comprehensive review on bio epoxy based IPN: synthesis, properties and applications, *Polymer* 252 (2022) 124950, <https://doi.org/10.1016/j.polymer.2022.124950>.
- [20] E. Piacenza, A. Presentato, R. Alduina, A. Scurria, M. Pagliaro, L. Albanese, F. Meneguzzo, R. Ciriminna, D.F. Chillura Martino, Cross-linked natural IntegroPectin films from citrus biowaste with intrinsic antimicrobial activity, *Cellulose* 29 (10) (2022) 5779–5802, <https://doi.org/10.1007/s10570-022-04627-1>.
- [21] T. Faddetta, G. Polito, L. Abbate, P. Alibrandi, M. Zerbo, C. Caldiero, C. Reina, G. Puccio, E. Vaccaro, M.R. Abenavoli, V. Cavaliere, F. Mercati, A. Palumbo Piccionello, G. Gallo, Bioactive metabolite survey of actinobacteria showing plant growth promoting traits to develop novel biofertilizers, *Metabolites* 13 (3) (2023) 374, <https://doi.org/10.3390/metabo13030374>.
- [22] L. Veneziano, V. Barra, D. Cilluffo, A. Di Leonardo, Proliferation of aneuploid cells induced by CENP-E depletion is counteracted by the p14ARF tumor suppressor, *Mol. Gen. Genomics.* 294 (1) (2019) 149–158, <https://doi.org/10.1007/s00438-018-1495-5>.
- [23] Z. Liu, S.Z. Erhan, Preparation of soybean oil polymers with high molecular weight, *J. Polym. Environ.* 18 (3) (2010) 243–249, <https://doi.org/10.1007/s10924-010-0179-y>.
- [24] Y. Su, S. Zhang, Y. Chen, T. Yuan, Z. Yang, One-step synthesis of novel renewable multi-functional linseed oil-based acrylate prepolymers and its application in UV-curable coatings, *Prog. Org. Coat.* 148 (2020) 105820, <https://doi.org/10.1016/j.porgcoat.2020.105820>.
- [25] J.F. Schmitz, S.Z. Erhan, B.K. Sharma, L.A. Johnson, D.J. Myers, 17 - Biobased products from soybeans, in: L.A. Johnson, P.J. White, R. Galloway (Eds.), *Soybeans*, AOC Press, 2008, pp. 539–612, <https://doi.org/10.1016/B978-1-893997-64-6.50020-2>.
- [26] P. Li, Z. Chu, Y. Chen, T. Yuan, Z. Yang, One-pot and solvent-free synthesis of castor oil-based polyurethane acrylate oligomers for UV-curable coatings applications, *Prog. Org. Coat.* 159 (2021) 106398, <https://doi.org/10.1016/j.porgcoat.2021.106398>.
- [27] A. Holmgren, G. Lindblom, L.B.A. Johansson, Intramolecular hydrogen bonding in a monoglyceride lipid studied by Fourier transform infrared spectroscopy, *J. Phys. Chem.* 92 (20) (1988) 5639–5642, <https://doi.org/10.1021/j100331a020>.
- [28] E.A. Disalvo, A.M. Bouchet, M.A. Frias, Connected and isolated CH<sub>2</sub> populations in acyl chains and its relation to pockets of confined water in lipid membranes as observed by FTIR spectrometry, *Biochim. Biophys. Acta Biomembr.* 1828 (8) (2013) 1683–1689, <https://doi.org/10.1016/j.bbmem.2013.02.007>.
- [29] M.-A. Poiana, E. Alexa, M.-F. Munteanu, R. Gligor, D. Moigradean, C. Mateescu, Use of ATR-FTIR spectroscopy to detect the changes in extra virgin olive oil by adulteration with soybean oil and high temperature heat treatment, *Open Chem.* 13 (1) (2015) 689–698, <https://doi.org/10.1515/chem-2015-0110>.

- [30] F. Pi, F. Kaneko, M. Iwahashi, M. Suzuki, Y. Ozaki, Solid-state low temperature → middle temperature phase transition of linoleic acid studied by FTIR spectroscopy, *J. Phys. Chem. B* 115 (19) (2011) 6289–6295, <https://doi.org/10.1021/jp200760p>.
- [31] P. Wolfangel, K. Müller, Chain order in lipid bilayers: FTIR and solid state NMR studies on bilayer membranes from 1,2-dimyristoyl-sn-glycero-3-phosphoglycerol, *J. Phys. Chem. B* 107 (36) (2003) 9918–9928, <https://doi.org/10.1021/jp0346920>.
- [32] F. Severcan, D.-O. Dorohoi, FTIR studies of temperature influence on the DPPG model membrane, *J. Mol. Struct.* 887 (1) (2008) 117–121, <https://doi.org/10.1016/j.molstruc.2008.02.039>.
- [33] R. Mendelsohn, M.A. Davies, J.W. Brauner, H.F. Schuster, R.A. Dluhy, Quantitative determination of conformational disorder in the acyl chains of phospholipid bilayers by infrared spectroscopy, *Biochemistry* 28 (22) (1989) 8934–8939, <https://doi.org/10.1021/bi00448a037>.
- [34] X. Zhao, D. Dong, W. Zheng, L. Jiao, Y. Lang, Discrimination of adulterated sesame oil using mid-infrared spectroscopy and chemometrics, *Food Anal. Methods* 8 (9) (2015) 2308–2314, <https://doi.org/10.1007/s12161-015-0125-7>.
- [35] T. Gocen, S.H. Bayari, M.H. Guven, Conformational and vibrational studies of arachidonic acid, light and temperature effects on ATR-FTIR spectra, *Spectrochim. Acta Part A* 203 (2018) 263–272, <https://doi.org/10.1016/j.saa.2018.05.100>.
- [36] V. Ciaramitaro, E. Piacenza, P.L. Meo, C. Librici, M.M. Calvino, P. Conte, G. Lazzara, D.F. Chillura Martino, From micro to macro: physical-chemical characterization of wheat starch-based films modified with PEG200, sodium citrate, or citric acid, *Int. J. Biol. Macromol.* 253 (2023) 127225, <https://doi.org/10.1016/j.ijbiomac.2023.127225>.
- [37] W. Liu, M.-E. Fei, Y. Ban, A. Jia, R. Qiu, Preparation and evaluation of green composites from microcrystalline cellulose and a soybean-oil derivative, *Polymers* 9 (10) (2017), <https://doi.org/10.3390/polym9100541>.
- [38] T. Tsujimoto, T. Takayama, H. Uyama, Biodegradable shape memory polymeric material from epoxidized soybean oil and polycaprolactone, *Polymers* 7 (10) (2015) 2165–2174, <https://doi.org/10.3390/polym7101506>.
- [39] J. Yang, Y.C. Ching, K.Y. Ching, X. Ran, N.M. Al-Hada, X. Sui, Y. Wei, S. Xu, J. Yu, J. Wang, J. Zhou, Preparation and characterization of starch-based bioplastic films modified by citric acid-epoxidized soybean oil oligomers, *J. Polym. Environ.* 31 (3) (2023) 954–964, <https://doi.org/10.1007/s10924-022-02661-5>.
- [40] P.-D. Hong, J.-H. Chen, Molecular aggregation behaviour of poly(vinyl chloride) solutions, *Polymer* 40 (14) (1999) 4077–4085, [https://doi.org/10.1016/S0032-3861\(98\)00629-6](https://doi.org/10.1016/S0032-3861(98)00629-6).
- [41] L.A. García-Cerda, M.U. Escareño-Castro, M. Salazar-Zertuche, Preparation and characterization of polyvinyl alcohol–cobalt ferrite nanocomposites, *J. Non-Cryst. Solids* 353 (8) (2007) 808–810, <https://doi.org/10.1016/j.jnoncrysol.2006.12.046>.
- [42] P.-D. Hong, J.-H. Chen, Structure and properties of polyvinyl chloride physical gels, *Polymer* 39 (3) (1998) 711–717, [https://doi.org/10.1016/S0032-3861\(97\)00350-9](https://doi.org/10.1016/S0032-3861(97)00350-9).
- [43] C. Rizzo, G. Misia, S. Marullo, F. Billeci, F. D'Anna, Bio-based chitosan and cellulose ionic liquid gels: polymeric soft materials for the desulfurization of fuel, *Green Chem.* 24 (3) (2022) 1318–1334, <https://doi.org/10.1039/D1GC02679H>.
- [44] C. Rizzo, S. Marullo, F. D'Anna, Carbon-based ionic liquid gels: alternative adsorbents for pharmaceutically active compounds in wastewater, *Environ. Sci. Nano* 8 (1) (2021) 131–145, <https://doi.org/10.1039/D0EN01042A>.
- [45] C. Rizzo, S. Marullo, P.R. Campodonico, I. Pibiri, N.T. Dintcheva, R. Noto, D. Millan, F. D'Anna, Self-sustaining supramolecular ionic liquid gels for dye adsorption, *ACS Sustain. Chem. Eng.* 6 (9) (2018) 12453–12462, <https://doi.org/10.1021/acssuschemeng.8b03002>.
- [46] M. Jain, A. Sahoo, D. Mishra, S. Aiman Khan, K. Kishore Pant, Z.M. Ziora, M.A. T. Blaskovich, Modelling and statistical interpretation of phenol adsorption behaviour of 3-dimensional hybrid aerogel of waste-derived carbon nanotubes and graphene oxide, *Chem. Eng. J.* 490 (2024) 151351, <https://doi.org/10.1016/j.cej.2024.151351>.
- [47] H. Song, K. Zhang, P. Li, G. Qin, W. Xiao, C. Zhang, Y. Zheng, Y. Ding, S. Ji, One-step construction of silver–polyaniline nanocomposite modified multifunctional sponges for wastewater remediation: adsorption, catalysis and antimicrobial applications, *J. Mater. Chem. A* 12 (11) (2024) 6747–6767, <https://doi.org/10.1039/D3TA07919H>.
- [48] G. Pi, Y. Li, M. Bao, L. Mao, H. Gong, Z. Wang, Novel and environmentally friendly oil spill dispersant based on the synergy of biopolymer Xanthan Gum and silica nanoparticles, *ACS Sustain. Chem. Eng.* 4 (6) (2016) 3095–3102, <https://doi.org/10.1021/acssuschemeng.6b00063>.
- [49] E. Khademian, E. Salehi, H. Sanaeepur, F. Galiano, A. Figoli, A systematic review on carbohydrate biopolymers for adsorptive remediation of copper ions from aqueous environments-part A: classification and modification strategies, *Sci. Total Environ.* 738 (2020) 139829, <https://doi.org/10.1016/j.scitotenv.2020.139829>.
- [50] P. Sirajudheen, P. Karthikeyan, S. Vigneshwaran, M. Nikitha, C.A.A. Hassan, S. Meenakshi, Ce(III) networked chitosan/β-cyclodextrin beads for the selective removal of toxic dye molecules: adsorption performance and mechanism, *Carbohydr. Polym. Technol. Appl.* 1 (2020) 100018, <https://doi.org/10.1016/j.carpta.2020.100018>.
- [51] M.V. Russo, I. Notardonato, A. Rosada, G. Ianiri, P. Avino, Halogenated volatile organic compounds in water samples and inorganic elements levels in ores for characterizing a high anthropogenic polluted area in the Northern Latium Region (Italy), *Int. J. Environ. Res. Public Health* 18 (4) (2021), <https://doi.org/10.3390/ijerph18041628>.
- [52] L.M. Saleh Medina, A. Cánavea, F.N. Molinari, N. D'Accorso, R.M. Negri, High removal of chlorinated solvents by reusable polydimethylsiloxane based adsorbents, *Polym. Eng. Sci.* 63 (2) (2023) 366–378, <https://doi.org/10.1002/pen.26211>.
- [53] C.C. dos Santos, R. Mouta, M.C.C. Junior, S.A.A. Santana, H.A.D.S. Silva, C.W. B. Bezerra, Chitosan-edible oil based materials as upgraded adsorbents for textile dyes, *Carbohydr. Polym.* 180 (2018) 182–191, <https://doi.org/10.1016/j.carbpol.2017.09.076>.
- [54] M.T. Dare, M. Bazmi, A. Khosravi, M. Monem, A. Jafari, H.A. Khonakdar, Soybean oil-based nanocomposites for dye adsorption: AESO-chitosan-graphene oxide synergy in water treatment, *Polym. Adv. Technol.* 35 (1) (2024) e6270, <https://doi.org/10.1002/pat.6270>.
- [55] Y. Gu, F. Jérôme, Bio-based solvents: an emerging generation of fluids for the design of eco-efficient processes in catalysis and organic chemistry, *Chem. Soc. Rev.* 42 (24) (2013) 9550–9570, <https://doi.org/10.1039/C3CS60241A>.
- [56] K.L. Law, R. Narayan, Reducing environmental plastic pollution by designing polymer materials for managed end-of-life, *Nat. Rev. Mater.* 7 (2) (2022) 104–116, <https://doi.org/10.1038/s41578-021-00382-0>.
- [57] F.M. Haque, J.S.A. Ishibashi, C.A.L. Lidston, H. Shao, F.S. Bates, A.B. Chang, G. W. Coates, C.J. Cramer, P.J. Dauenhauer, W.R. Dichtel, C.J. Ellison, E.A. Gormong, L.S. Hamachi, T.R. Hoyer, M. Jin, J.A. Kalow, H.J. Kim, G. Kumar, C.J. LaSalle, S. Liffland, B.M. Lipinski, Y. Pang, R. Parveen, X. Peng, Y. Popowski, E. A. Prebhalo, Y. Reddi, T.M. Reineke, D.T. Sheppard, J.L. Swartz, W.B. Tolman, B. Vlaisavljevich, J. Wissinger, S. Xu, M.A. Hillmyer, Defining the macromolecules of tomorrow through synergistic sustainable polymer research, *Chem. Rev.* 122 (6) (2022) 6322–6373, <https://doi.org/10.1021/acs.chemrev.1c00173>.
- [58] T. Gocen, S. Haman Bayari, M. Haluk Guven, Linoleic acid and its potassium and sodium salts: a combined experimental and theoretical study, *J. Mol. Struct.* 1150 (2017) 68–81, <https://doi.org/10.1016/j.molstruc.2017.08.065>.
- [59] W.Q. Gong, A. Parentich, L.H. Little, L.J. Warren, Adsorption of oleate on apatite studied by diffuse reflectance infrared Fourier transform spectroscopy, *Langmuir* 8 (1) (1992) 118–124, <https://doi.org/10.1021/la00037a023>.
- [60] H. Staiger, K. Staiger, N. Stefan, H.G.N. Wahl, F. Machicao, M. Kellerer, H.-U. Häring, Palmitate-induced interleukin-6 expression in human coronary artery endothelial cells, *Diabetes* 53 (12) (2004) 3209–3216, <https://doi.org/10.2337/diabetes.53.12.3209>.
- [61] C.J. Urso, H. Zhou, Palmitic acid-induced defects in cell cycle progression and cytokinesis in Neuro-2a cells, *Cell Cycle* 21 (10) (2022) 1048–1057, <https://doi.org/10.1080/15384101.2022.2040769>.